GOODS-ALMA 2.0: Last gigayear star formation histories of the so-called starbursts within the main sequence

L Ciesla, C Gómez-Guijarro, V Buat, D Elbaz, S Jin, M Béthermin, E Daddi, M Franco, H Inami, G Magdis, et al.

A&A 672, A191 (2023)
https://doi.org/10.1051/0004-6361/202245376

Astronomy & Astrophysics

GOODS-ALMA 2.0: Last gigayear star formation histories of the so-called starbursts within the main sequence

L. Ciesla[1], C. Gómez-Guijarro[2], V. Buat[1,3], D. Elbaz[2], S. Jin[4,5,6], M. Béthermin[1], E. Daddi[2], M. Franco[7], H. Inami[8], G. Magdis[4,5,6], B. Magnelli[2], and M. Xiao[9]

[1] Aix-Marseille Univ., CNRS, CNES, LAM, 13388 Marseille Cedex 13, France
[2] Université Paris-Saclay, Université Paris Cité, CEA, CNRS, AIM, 91191 Gif-sur-Yvette, France
e-mail: laure.ciesla@lam.fr
[3] Institut Universitaire de France (IUF), Paris, France
[4] Cosmic Dawn Center (DAWN), Copenhagen, Denmark
[5] DTU-Space, Technical University of Denmark, Elektrovej 327, 2800 Kgs. Lyngby, Denmark
[6] Niels Bohr Institute, University of Copenhagen, Jagtvej 128, 2200 Copenhagen N, Denmark
[7] Department of Astronomy, The University of Texas at Austin, 2515 Speedway Blvd Stop C1400, Austin, TX 78712, USA
[8] Hiroshima Astrophysical Science Center, Hiroshima University, 1-3-1 Kagamiyama, Higashi-Hiroshima, Hiroshima 739-8526, Japan
[9] School of Astronomy and Space Science, Nanjing University, Nanjing 210093, PR China

Received 4 November 2022 / Accepted 10 February 2023

ABSTRACT

Recently, a population of compact main sequence (MS) galaxies exhibiting starburst-like properties were identified in the GOODS-ALMA blind survey at 1.1 mm. Several evolution scenarios were proposed to explain their particular physical properties (e.g., compact size, low gas content, short depletion time). In this work, we aim to study the star formation history (SFH) of the GOODS-ALMA galaxies to understand whether or not the so-called 'starbursts (SBs) in the MS' galaxies exhibit a star formation activity over the last gigayear that is different from that of the MS galaxies and that could explain their specificity. We use the CIGALE SED modelling code to which we add nonparametric SFHs. To compare the recent SFHs of the galaxies quantitatively, we define a parameter, the star formation rate (SFR) gradient, which provides the angle showing the direction that a galaxy has followed in the SFR-versus-stellar-mass plane over a given period. We show that SB in the MS galaxies show positive or weak negative gradients over the last 100, 300, and 1000 Myr, which is at odds with a scenario where these galaxies would be transitioning from the SB region at the end of a strong starburst phase. Normal GOODS-ALMA galaxies and "SB in the MS" galaxies show the same SFR gradient distribution, meaning that they have similar recent SFHs despite their different properties (compactness, low depletion time). The "SBs in the MS" galaxies manage to maintain their star-formation activity, allowing them to stay within the MS. This points toward a diversity of galaxies within a complex MS.

Key words. galaxies: evolution – galaxies: fundamental parameters

1. Introduction

The discovery of a tight relation between the star formation activity of galaxies and their stellar mass was a significant new development in our understanding of galaxy evolution (Noeske et al. 2007; Elbaz et al. 2007). One of the main consequences of this relation is that galaxies form the bulk of their stars through secular processes rather than violent episodes of star formation. This relation between the star formation rate (SFR) and stellar mass (M_*), the so-called galaxies main sequence (MS), has now been constrained up to $z \sim 5$ (e.g., Schreiber et al. 2018a; Khusanova et al. 2021; Topping et al. 2022) and its slope and normalisation vary with cosmic time (e.g., Speagle et al. 2014; Schreiber et al. 2015; Leja et al. 2021). However, what is striking is that the dispersion of the MS relation seems to be constant whatever the stellar mass range or redshift studied (e.g., Guo et al. 2013; Schreiber et al. 2015); although Leja et al. (2021) recently claimed a wider MS at redshifts of higher than 2 and at the high mass end ($\sim 10^{11}\ M_\odot$). Several studies have shown that there is a coherent variation of the physical properties of galaxies within the MS, such as the gas fraction (Magdis et al. 2012; Wuyts et al. 2011; Salmi et al. 2012; Saintonge & Catinella 2022), suggesting that the scatter of the MS is the result of physical processes rather than uncertainties on the measurements. However, the path that galaxies follow on the SFR–M_* diagram and the processes that drive these evolutionary paths are still debated.

Studying the properties of star forming galaxies within the scatter of the MS is of paramount importance to our understanding of the mechanisms governing smooth and self-regulated galaxy evolution. Recent studies using the Atacama Large Millimeter/submillimeter array (ALMA) have highlighted the existence of a population of starburst (SB) galaxies within the scatter of the MS. These sources have short depletion timescales and enhanced star-formation surface densities, and exhibit compact star formation traced by submillimeter and millimeter (submm/mm) dust continuum emission (Elbaz et al. 2018) or by radio emission (Jiménez-Andrade et al. 2019), hence their name. Constraints on the evolutionary scenario of these populations of compact galaxies and 'SB in the MS' galaxies have yet to be

obtained. Several studies have advocated for compaction events predicted by galaxy-formation models, in which extended star-forming galaxies in the MS can secularly evolve into compact star-forming galaxies in the MS by funneling gas to their central regions, yielding the build up of their stellar cores (e.g., Dekel et al. 2013; Zolotov et al. 2015; Tacchella et al. 2016). Others have proposed a funneling of the gas to the center, driven by a violent episode of star formation typical of gas-rich mergers (e.g., Mihos & Hernquist 1996; Hopkins et al. 2006; Toft et al. 2014; Gómez-Guijarro et al. 2018; Puglisi et al. 2021). In this scenario, compact star-forming galaxies in the MS would then be at the end of their starbursting phase, having consumed most of their gas, and be just passing through the MS on their way to quiescence (Elbaz et al. 2018; Gómez-Guijarro et al. 2019; Puglisi et al. 2021).

Studying the galaxies detected in the blind GOODS-ALMA 2.0 survey (Gómez-Guijarro et al. 2022a), Gómez-Guijarro et al. (2022b) showed that the 'SB in the MS' are extreme cases where the dust continuum areas are the most compact ones, and are associated with the shortest depletion timescales, lowest gas fractions, and the highest dust temperatures, compared to typical main sequence GOODS-ALMA star-forming galaxies at the same stellar mass and redshift. Following Elbaz et al. (2018), Gómez-Guijarro et al. (2022b) defined 'starbursts (SBs) in the MS' galaxies as those that are within a 0.5 dex dispersion relative to the Schreiber et al. (2015) MS and have a depletion timescale below the scatter of the relation of Tacconi et al. (2018). Gómez-Guijarro et al. (2022b) suggest that their star formation rate is somehow sustained in very massive star-forming galaxies, keeping them within the MS even when their gas fractions are low. These authors claim that these galaxies are presumably on their way to quiescence.

To be able to put a constraint on the evolutionary path of these galaxies, we must be able to reconstruct the star formation history (SFH) of galaxies in general. In the absence of SFH tracers from emission and/or absorption emission lines, SFH recovery must rely on spectral energy distribution (SED) modelling of continuum emission. Although the parametric SFH can be used to derive the physical properties of galaxies, it suffers from strong bias, which prevents a correct reconstruction of the SFH (see e.g., Buat et al. 2014; Ciesla et al. 2015, 2017; Carnall et al. 2019; Lower et al. 2020; Leja et al. 2021). Several methods making use of parametric SFHs have been developed to at least put constraints on the last few hundreds million years of the SFH using, for instance, the Bayesian information criterion (BIC, Ciesla et al. 2018) or approximate Bayesian computation (ABC, Aufort et al. 2020; Ciesla et al. 2021). However, to go back further in time, parametric SFH can no longer be used and more advanced SFH formulation must be taken into account. Non-parametric SFHs have been proposed to break free from the degeneracies and biases produced by parametric SFHs (e.g., Iyer & Gawiser 2017; Iyer et al. 2019; Leja et al. 2019; Lower et al. 2020) and have been implemented in several SED modelling codes such as `Prospector` (Leja et al. 2017; Johnson et al. 2021) and `Bagpipes` (Carnall et al. 2018).

In this paper, we aim to investigate the SFH of GOODS-ALMA galaxies, in particular the "SB in the MS" galaxies to understand if the extreme properties they exhibit can be explained by the history of their star formation activity. To reach this goal, we implement in `CIGALE` non-parametric SFHs and test their accuracy and sensitivity to recent SFH variations. We use this approach to reconstruct the last gigayear of the SFH of GOODS-ALMA galaxies. This article is structured as follows: The GOODS-ALMA sample is described in Sect. 2. We detail the SED modelling procedure in Sect. 3, including the addition of non-parametric SFHs and tests on their sensitivity. Results from SED modelling and the analysis of the recent SFH of GOODS-ALMA galaxies are provided in Sect. 4. A discussion of these results and the conclusion of the paper are detailed in Sects. 5 and 6, respectively. Throughout the paper, we use a Salpeter (1955) initial mass function.

2. The GOODS-ALMA sample

GOODS-ALMA is a blind 1.1 mm galaxy survey of the deepest part of the Great Observatories Origins Deep Survey South (GOODS-South; Dickinson et al. 2003; Giavalisco et al. 2004) field. The survey covers a continuous area of 72.42 arcmin^2 with ALMA Band 6 observations using two array configurations, providing high- and low-angular-resolution datasets at a homogenous average sensitivity (programs 2015.1.00543.S and 2017.1.00755.S; PI: D. Elbaz). The high-resolution dataset was presented in Franco et al. (2018; GOODS-ALMA 1.0), while the low-resolution dataset and its combination with the high resolution was presented in Gómez-Guijarro et al. (2022a; GOODS-ALMA 2.0). The combined mosaic reaches an average point-source sensitivity of 68.4 μJy beam^{-1} at an average angular resolution of $0.447'' \times 0.418''$. We refer the reader to Franco et al. (2018) and Gómez-Guijarro et al. (2022a) for details of the survey observations, data processing, and source catalogue.

In this work, we use the GOODS-ALMA 2.0 source catalogue presented in Gómez-Guijarro et al. (2022a,b), which is composed of 88 sources. In particular, we focus on the subset of galaxies with a *Herschel* counterpart (69/88), as presented in Gómez-Guijarro et al. (2022b), but discarding galaxies labelled as optically dark or faint (also known as HST-dark) in the GOODS-ALMA 2.0 catalogue. The sample is composed of 65 galaxies with continuous ultraviolet (UV) to mm photometry coverage, which is needed for the purpose of this work. In the following, we adopt the redshifts reported in the GOODS-ALMA 2.0 source catalogue.

Ultraviolet and near-infrared (near-IR) photometry are taken from the ASTRODEEP-GS43 (Merlin et al. 2021) catalogue. This catalogue provides updated consistent photometry measurements in 43 optical and IR bands (25 wide and 18 medium filters) ranging from *U*-band to *Spitzer*/IRAC/8 μm in the GOODS-South field. Additionally, we employ mid-IR to mm data, including *Spitzer*/MIPS/24 μm images from GOODS; *Herschel*/PACS/70, 100, and 160 μm from GOODS-*Herschel* (Elbaz et al. 2011) and PEP (Lutz et al. 2011) combined (Magnelli et al. 2013); *Herschel*/SPIRE/250, 350, and 500 μm from HerMES (HerMES Collaboration 2012); and ALMA 1.1 mm from GOODS-ALMA 2.0 (Gómez-Guijarro et al. 2022a). We refer the reader to Gómez-Guijarro et al. (2022b) for further details of the photometry at these wavelengths.

3. The SED modelling procedure

3.1. Inclusion of non-parametric star formation histories in `CIGALE`

We use the SED modelling code `CIGALE`[1] (Boquien et al. 2019), which combines a set of modules modelling the SFH, the emission of the stellar populations, the attenuation from dust, the

[1] https://cigale.lam.fr/

dust emission, and the AGN contribution from X-ray to radio. Regarding the SFH, two main approaches are already implemented in CIGALE. The first is the possibility of using any file containing an SFH, such as the output of a simulation for instance. The second approach is to use a parametric model, such as an exponentially declining or rising SFH, or τ-delayed SFH, adding a recent burst or quenching. In this study, we add a third possibility: a non-parametric set of SFHs. For this, we use the 2022.1 version of CIGALE customised for the purpose of this work.

Contrary to the parametric SFHs, the non-parametric SFHs do not assume any analytic function to model the SFH. This approach assumes a given number of time bins in which the SFRs are constant. We take advantage of the versatility of CIGALE and implement a new SFH module, SFHNLEVELS. Based on the results of Ocvirk et al. (2006), Leja et al. (2019) defined seven redshift bins in lookback time [0, 30, 100, 330, 1100, 3600, 11 700, 13 700] (in Myr). The number and time limits of these bins were extensively tested by Leja et al. (2019) and used in further works (e.g., Leja et al. 2021; Tacchella et al. 2020, 2021b; Lower et al. 2020). As in the other SFH modules of CIGALE, the age of the galaxy is a free parameter. For each age value, the time interval is divided into seven bins, conserving the logarithmic scaling used in Leja et al. (2019). The first bin age is fixed and defined as an input parameter. The limits of the time bins are therefore only dependent on the input values of the age provided to CIGALE before a run.

To link the SFR of each bin and prevent the computation of unrealistic SFHs, we use a prior that weights against sharp transitions between the SFH bins. Several studies have tested different priors such as Dirichlet or continuity for instance (Leja et al. 2019; Lower et al. 2020; Tacchella et al. 2020, 2021b; Suess et al. 2022). We choose to implement the bursty continuity (see for instance Tacchella et al. 2021b) in CIGALE, as in light of the results of these studies, this offers the best compromise in terms of accuracy in retrieving the stellar mass and SFR of galaxies. More specifically, the continuity prior is a Student-t distribution for the prior $x = \log(\mathrm{SFR}_n/\mathrm{SFR}_{n+1})$:

$$\mathrm{PDF}(x,\nu) = \frac{\Gamma(\frac{\nu+1}{2})}{\sqrt{\nu\pi}\Gamma(\frac{1}{2}\nu)}\left(1+\frac{(x/\sigma)^2}{\nu}\right)^{-\frac{\nu+1}{2}}, \quad (1)$$

where Γ is the γ function, σ a scale factor controlling the width of the distribution, and ν the degree of freedom controlling the probability in the tails of the distribution. We choose to adopt $\nu = 2$ following Leja et al. (2019) and $\sigma = 1$ following Tacchella et al. (2021b). Indeed, as shown in Tacchella et al. (2021b), this prior will allow us to reach a wider range of specific SFR (sSFR) compared to the simple continuity prior with $\nu = 2$. In the SFHNLEVELS module, the SFR of the first bin is set to 1, and the SFRs of the following bins are then obtained by randomly choosing x in the Students-t distribution. The obtained SFH is then normalised to 1 $M_\odot$ and used to build the modelled SED. CIGALE provides output parameters obtained from the best-fit models as well as derived from a Bayesian-like analysis, that is, computed from the probability distribution function (PDF) of a given parameter. The SFR in each bin can be obtained from the PDF analysis as well. The age of formation, age_{form}, which is the time at which the galaxy has formed half of its stellar mass is also an output of the module.

3.2. Accuracy of the non-parametric SFH

We test the ability of non-parametric SFHs to model the SED of galaxies using a set of 100 SFHs of simulated $z = 1$ typical main sequence galaxies obtained with the semi-analytical code GALFORM (Cole et al. 2000; Bower et al. 2006; Benson & Bower 2010) already used in Ciesla et al. (2015) to test several parametric SFHs. CIGALE is used to produce SEDs associated to the GALFORM SFHs assuming different models. In this test, to focus only on the effect of the SFH model used to perform the SED fitting, we build and fit the SED using the same single stellar population model (Bruzual & Charlot 2003), attenuation law (Calzetti et al. 2000), and dust emission (Dale et al. 2014). This test was carried out by Ciesla et al. (2015) to quantify the ability of exponential and τ-delayed SFHs to recover the stellar mass and SFR of simulated galaxies. To be able to compare their results with ours, we built mock galaxy SEDs associated with the GALFORM SFHs using the same set of parameters. We then ran CIGALE using a τ-delayed plus flexibility SFH as our fiducial parametric SFH. This model has been proposed in recent studies to decouple the long-term SFH from the recent SF activity by allowing an additional flexibility to the τ-delayed SFH (Ciesla et al. 2017; Schreiber et al. 2018b; Małek et al. 2018). We then ran CIGALE using the non-parametric SFH.

The results are shown in Fig. 1 for the stellar mass and SFR. The τ-delayed+flex SFH clearly underestimates the stellar mass of the GALFORM galaxies with a mean shift of $-18.9 \pm 6.5\%$ while the SFR is well recovered with an offset compared to the true value of $-4.0 \pm 6.7\%$. These results are consistent with those of Lower et al. (2020) and Iyer & Gawiser (2017), who also found an underestimation of the stellar mass and a good estimate of the SFR from the τ-delayed + burst SFH. When using the non-parametric SFH, the offset regarding the stellar mass is more dispersed, but is more centred around the true value ($3.0 \pm 3.6\%$). The SFR is also well recovered, with a mean offset of $4.7 \pm 3.3\%$. These results are consistent with those of Leja et al. (2021), who obtained larger stellar masses than SED fitting methods using parametric assumptions for the SFH as well.

We now consider the results of the analysis of Ciesla et al. (2015; see their Table 4), who tested the '1-exponentially' declining and '2-exponentially' declining SFHs as well as the canonical τ-delayed SFH. Both the τ-delayed+flex and non-parametric SFHs tested in this work provide good results (less than 5% error) in terms of SFR compared to the SFHs tested in Ciesla et al. (2015). However, in terms of stellar mass, the non-parametric SFH yields the best stellar mass estimates (Fig. 1). As the GALFORM SFHs show some strong and rapid variations over the life of the galaxies – changes that are quite drastic – we repeated the test, smoothing the GALFORM SFHs over 500 Myr and 1 Gyr, and found consistent results. The results of these tests show that the non-parametric SFHs provide a more accurate estimate of the stellar mass of galaxies than parametric models, which tend to provide underestimated results.

3.3. Sensitivity of the non-parametric SFH

In this work, we aim to identify any recent variation of star-formation (SF) activity that GOODS-ALMA galaxies may have undergone in the last few hundred million years. Therefore, we need to assess the ability of the non-parametric SFHs to recover such variations. When introducing the non-parametric SFHs, Leja et al. (2019) tested them on several simple cases including

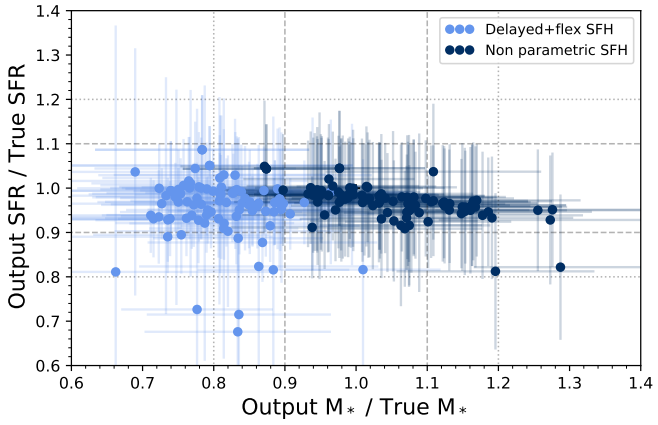

Fig. 1. Comparison between the physical properties (stellar masses and SFRs) obtained by CIGALE and the true properties of the GALFORM simulated galaxies. Results are compared using a τ-delayed SFH (light blue points) and non-parametric SFH (dark blue points).

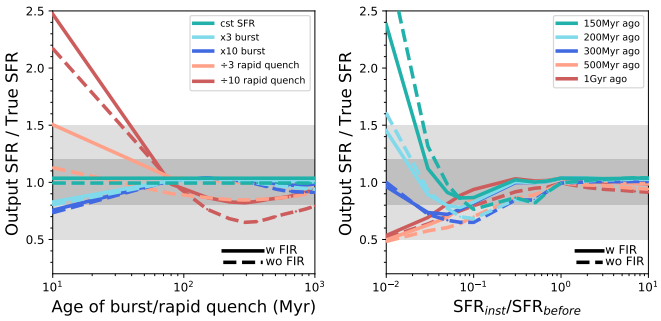

Fig. 2. Sensitivity of the non-parametric SFH in recovering rapid and recent variation of SFH. In both panels, the y-axis indicates the ratio between the estimated SFR obtained from the non-parametric SFH and the true one. The variation of this ratio is shown as a function of the age of the rapid variation (left panel) and its strength, which is the ratio between the instantaneous SFR and the SFR before the burst or quenching (right panel). In both panels, the solid line represents the results obtained when the full observed UV–mm SED is fitted and the dashed line shows results from when no FIR data are used for the fit.

a burst and a sudden quench. However, in their test, the sudden quench occurred 1 Gyr ago and they found that the continuity prior provides a good estimate of the SFR. We try to refine the test to see the limits of the SFH sensitivity. As we adopt the bursty continuity prior (Tacchella et al. 2021a) we evaluate the extent to which we can recover this burstiness.

To perform our test, we simulate a set of mock SEDs with CIGALE. We assume a constant SFH with a final instantaneous burst or quenching. The time when this instantaneous variation occurs varies from 10 Myr to 1 Gyr. Its strength, which is the ratio between the actual SFR and the SFR just before the variation, is set to between 0.01 and 10 in order to probe both strong quenching and strong starburst. The mock SEDs are then integrated into the GOODS-ALMA set of filters and fluxes are randomly perturbed using a Gaussian distribution with a standard deviation of 10% of the flux density in each filter. We used CIGALE to fit this mock catalogue using non-parametric SFH and show the results of this test in Fig. 2. If the SFH is constant or just underwent a rapid burst, even a factor ten starburst, the SFR is well recovered regardless of when this burst occurred. However, for starburst events, we note that the recovered SFR starts to be underestimated by between a few percent and 20% if this

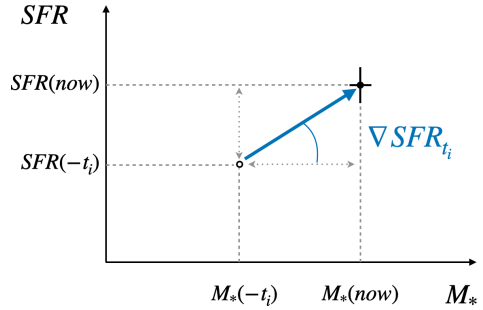

Fig. 3. Diagram explaining the definition of the SFR gradient. Using the output SFH from CIGALE, the SFR and M_* obtained t_i Myr ago are used to place the galaxy at the position where it was t_i Myr ago on the SFR–M_* plane. The SFR gradient is the angle between the line linking the position of the galaxy t_i Myr ago and its position now and the line drawn from a constant SFR.

variation happened less that 30 Myr ago. Regarding rapid quenching events, the SFR is slightly underestimated if the quenching happened between 100 Myr and 1 Gyr ago. Below 100 Myr, the SFR starts to be overestimated by 50% if the quenching happened between 40 and 100 Myr ago, and by a factor of up to 2.5 for more recent quenching events. We note that for these variations, the true SFR is set close to 0 and a factor 2.5 overestimate keeps this value very low and therefore does not lead to bias in favour of an active SFR. We perform this test with and without using the FIR filters, and find no significant difference in the results.

3.4. Definition of the SFR gradient

For the purpose of this work, we also compute a new parameter, the SFR gradient, ∇SFR. This parameter provides the angle showing the direction that a galaxy has followed in the usual representation of the MS, that is, the SFR versus stellar mass plane, during a given time (this time is an input free parameter) associated to the modelled SFH. In other words, the SFR gradient is the angle between the line linking the position of the galaxy t_i Myr ago and its position now and the line drawn from a constant SFR (Fig. 3). A value close to zero° means that the recent SFH is constant overall with no sharp variation. However, a large positive or negative value would mean that the galaxy undergoes a starburst or quenching phase. The SFR gradient allows us to perform a quantitative analysis of the recent SFH of galaxies and see the movements of galaxies relative to the MS.

4. Results from SED modelling

We ran CIGALE on the GOODS-ALMA sample using the SFHNLEVELS SFH module, stellar populations models of Bruzual & Charlot (2003), a modified Calzetti et al. (2000) starburst attenuation law module, and the Dale et al. (2014) IR templates. The parameters used for the two runs are provided in Table 1. The code uses energy balance to fit the entire SED from UV to submm, as we rely on the results of Seillé et al. (2022) who tested it extensively on the highly perturbed and star-forming Antennae system. These authors showed that the results of the UV-submm SED modelling of the entire system using energy balance are consistent with the sum of the results of the UV-submm SED modelling of individual regions, although they exhibit highly different levels of attenuation.

In terms of results, CIGALE provides the output values of the parameters computed from the Bayesian-like analysis. The

Table 1. CIGALE input parameters used to fit the GOODS-ALMA sample.

Parameter	Value	
Non-parametric SFH – SFHNLEVELS		
age (Gyr)	[1.2; 8.7]	10 values linearly sampled
$N_{\rm SFH}$	10 000	# of SFH per *age* value
First bin age	30 Myr	
Dust attenuation – DUSTATT_MODIFIED_STARBURST		
$E(B-V)$s lines	[0; 1.5]	14 values linearly sampled
$E(B-V)$s factor	1	
Dust emission – Dale et al. (2014)		
α	1, 1.5, 2, 2.5, 3	

Notes. This set of parameters resulted in 378 000 SED models.

output value of a parameter is the mean of its PDF, assuming that it is Gaussian, and the error is the standard deviation of the PDF. Parameters linked to the SFH are known to be difficult to constrain (see e.g., Buat et al. 2015; Ciesla et al. 2017; Carnall et al. 2019). Therefore, to go a step further and obtain more robust results, we performed an additional step in our estimate of the physical parameters of the GOODS-ALMA galaxies. For each galaxy, we added random noise assuming a Gaussian distribution with $\sigma = 0.1 \times S_\nu$ to the flux of each band, and repeated the operation ten times. Therefore, each galaxy was fitted ten times with CIGALE. The final value of a parameter is the mean value of the ten Bayesian output values, and the error is the dispersion of these ten Bayesian output values.

4.1. Mock analysis

As a standard procedure, we analyse the ability of the code to constrain the key parameters necessary to this study. The mock analysis procedure has been extensively described in previous works (e.g., Buat et al. 2019; Boquien et al. 2019; Ciesla et al. 2021). Although its principle is the same as in the tests performed in Sects. 2 and 3.2, the difference here is that the mock SEDs are created using the SED fit of the GOODS-ALMA galaxies of our sample. The best models of this first run are used as mock galaxies representative of the GOODS-ALMA population for which all parameters are known. Thus, the input parameters are representative of our galaxy population. A second run of CIGALE is used to see how well we constrain these parameters. The results of the mock analysis are shown in Fig. 4 for the key parameters used in this study. The output values are computed using the new method described in the previous section. A one-to-one relationship between the true values and the estimated ones implies a perfect constraint of the parameter.

As expected given the wavelength range covered by the GOODS-ALMA set of filters, the stellar mass, SFR, and dust attenuation are well recovered. Regarding the parameters linked to the SFH, the formation age of the galaxies is relatively well constrained. Usually, galaxy age is a parameter that is difficult to constrain and can be found fixed in several papers in the literature (see e.g., Ciesla et al. 2021). The SFR in the first SFH bin is well constrained, while the SFR is more difficult to constrain in the older bins. In the second and third bins of SFH, only the high SFR values are well recovered. The SFR of bin 4 seems to be constrained as well, although the relation is more dispersed. Regarding the SFR gradient, the relations are dispersed but do not show strong bias. Positive gradients are recovered positive and negative gradients are recovered negative. A few galaxies show some discrepancies, but for the purpose of this work, being able to differentiate between increasing and decreasing SF activities is sufficient. In conclusion, the constraints on the SFR, M_*, and SFR gradients allow us to conduct our analysis.

4.2. Physical parameters

All redshifts included, from 0.12 to 4.73, the mean stellar M_* estimated with CIGALE is $1.3 \times 10^{11}\,M_\odot$, with values ranging from 1.1×10^9 to $4.7 \times 10^{11}\,M_\odot$. We compare our stellar masses and SFR estimates to the values used in Gómez-Guijarro et al. (2022b) in Fig. 5. There is a significant scatter in the estimate of the stellar mass. On average, we find larger stellar masses with a median ratio of 1.26, which is expected, and a standard deviation of 2.14. Indeed, Leja et al. (2021) showed that using non-parametric SFH results in larger stellar mass estimates. This is due to the fact that parametric SFH are rigid and in order to provide a good fit and estimates of the SFR, the estimated age of the galaxies is younger (see also, Ciesla et al. 2017; Carnall et al. 2019). Our results on GOODS-ALMA galaxies confirm what we obtained from simulations in Sect. 3.1 and the results of Leja et al. (2021). Regarding the SFR, it is on average lower than the estimates from Gómez-Guijarro et al. (2022b) with a median ratio of 0.40 and a dispersion of 0.35. This is due to the fact that CIGALE takes into account the IR emission due to dust heated by older stellar populations, resulting in lower SFR compared to UV+IR inferred values, a conclusion also reached by Leja et al. (2021).

4.3. The recent SFH of GOODS-ALMA galaxies

We now look at the recent SFH obtained for the GOODS-ALMA galaxies. We emphasise that the SFRs and stellar masses used hereafter are those obtained by the CIGALE SED fitting and not the values used by Gómez-Guijarro et al. (2022b). However, we keep the 'SB in the MS' sample defined by Gómez-Guijarro et al. (2022b) in order to discuss the SFH properties of these particular sources. We reiterate that 'SB in the MS' galaxies are defined as those that are within a 0.5 dex dispersion relative to the Schreiber et al. (2015) MS and have a shorter depletion timescale than the scatter of the relation of Tacconi et al. (2018). We note that, due to the uncertainties in the relevant quantities (SFR, gas mass, and stellar mass), the subset of 'SB in the MS' galaxies could vary, as some enter or exit the selection criteria. In order to mitigate this effect, we also note that the definition is for galaxies with shorter depletion timescales than the scatter of the scaling relation including their error bars.

In Fig. 6, we place these sources relative to the Schreiber et al. (2015) MS as a function of their stellar mass. Galaxies are colour coded according to their SFR gradient obtained over 100, 300, and 1000 Myr. The arrows are a visual indication of these gradients; those with a black edge indicate galaxies classified as SB in the MS by Gómez-Guijarro et al. (2022b). These arrows provide a hint as to the movement of the galaxies on the SFR–M_* plane. To obtain information about the difference in terms of SED shape for two extreme gradient values, we show the best SED fit of A2GS26 and A2GS50 in Fig. 7, which show a SFR gradient over 100 Myr of −48° and 60°, respectively. The two SEDs are shown in rest-frame wavelength and are normalised to their flux density at 2 µm rest frame – a proxy for stellar mass – to facilitate the comparison. The SED of A2GS26, which has the smallest gradient, shows a decline in UV

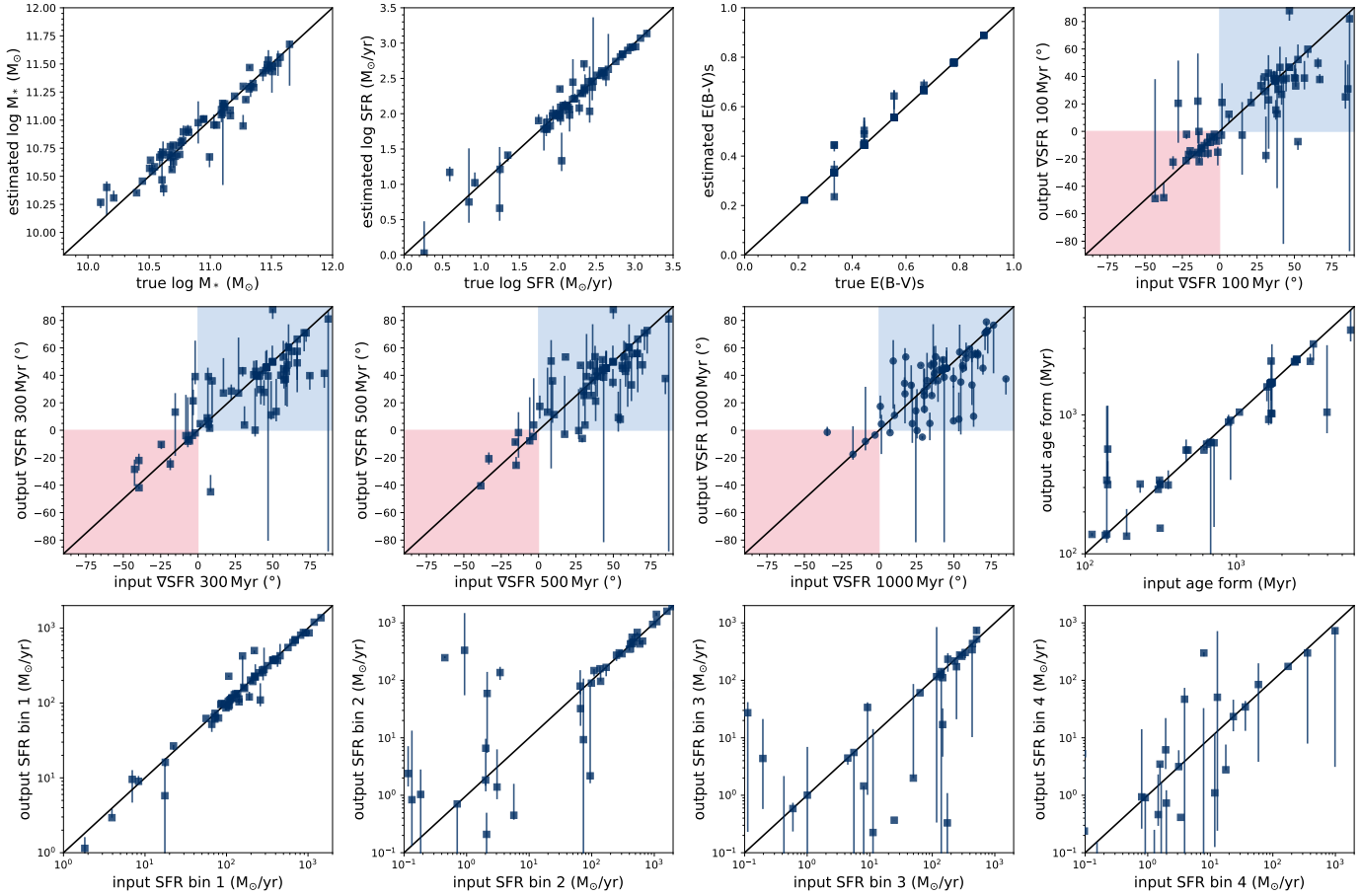

Fig. 4. Results of the mock analysis built from the GOODS-ALMA galaxies for the key parameters used in this work. The black solid line is the one-to-one relationship.

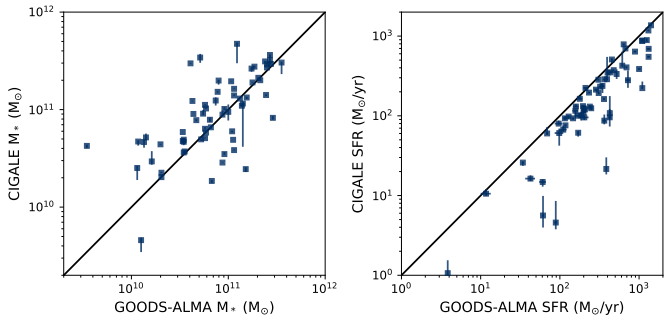

Fig. 5. Comparison between the stellar mass and SFR values of the GOODS-ALMA sample provided in Gómez-Guijarro et al. (2022b) and those obtained with CIGALE using a non-parametric SFH.

emission, a strong Balmer break, and weaker IR emission compared to A2GS50. All of these are signs of decreasing star formation activity.

In the top panel of Fig. 6, gradients are measured over 100 Myr. The GOODS-ALMA galaxies exhibit a wide range of gradients, mostly larger than −25°. This timescale reveals the stochastic variations of the recent SFH. We can distinguish mainly two groups separated in mass. Galaxies of the first group with masses lower than $5 \times 10^{10}\,M_{\odot}$ are mostly located in the upper part of the MS, in the light grey region. No galaxies are found in the centre of the MS scatter or in the lower part. This is due to the detection limit implied by the GOODS-ALMA blind survey. Four of these galaxies are located in the SB region, at a factor of 5 above the MS. This 'low'-mass group of galaxies have a positive gradient indicative of an undergoing enhanced star-formation activity. However, a few of them exhibit a flatter gradient that could indicate a slow decline or constant star formation over the last 100 Myr. Galaxies defined as 'SB in the MS' display both strong and flatter gradients. Using the SFR estimated by CIGALE with the non-parametric SFH, all but one of these galaxies are located within the MS. At higher masses, above $5 \times 10^{10}\,M_{\odot}$, the GOODS-ALMA galaxies lie within the MS, in its lower part or below. A wider spread of gradients is observed among these sources, showing a large range of SFHs. Galaxies classified as 'SB in the MS' share this wide distribution of gradients with the normal GOODS-ALMA galaxies. Errors on the discussed gradients are provided in Fig. 8, where we show the 1σ superior and inferior errors on the gradients. These are the errors seen in Fig. 4. The results of Fig. 6 are not affected by the errors on the estimates of the gradient parameters.

The GOODS-ALMA blind survey is a 1.1 mm flux-limited survey. We refer the reader to Gómez-Guijarro et al. (2022a,b) for a full discussion of flux completeness limits and how these map into limits on the gas masses and depletion timescales. Briefly, the flux detection limit implies that the survey selection effects go against finding galaxies with low gas masses at fixed redshift, stellar mass, and SFR, and therefore against galaxies with short depletion timescales, such as those classified as 'SB in the MS'. Galaxies not detected in the GOODS-ALMA sample will therefore start populating the MS in the low-mass end.

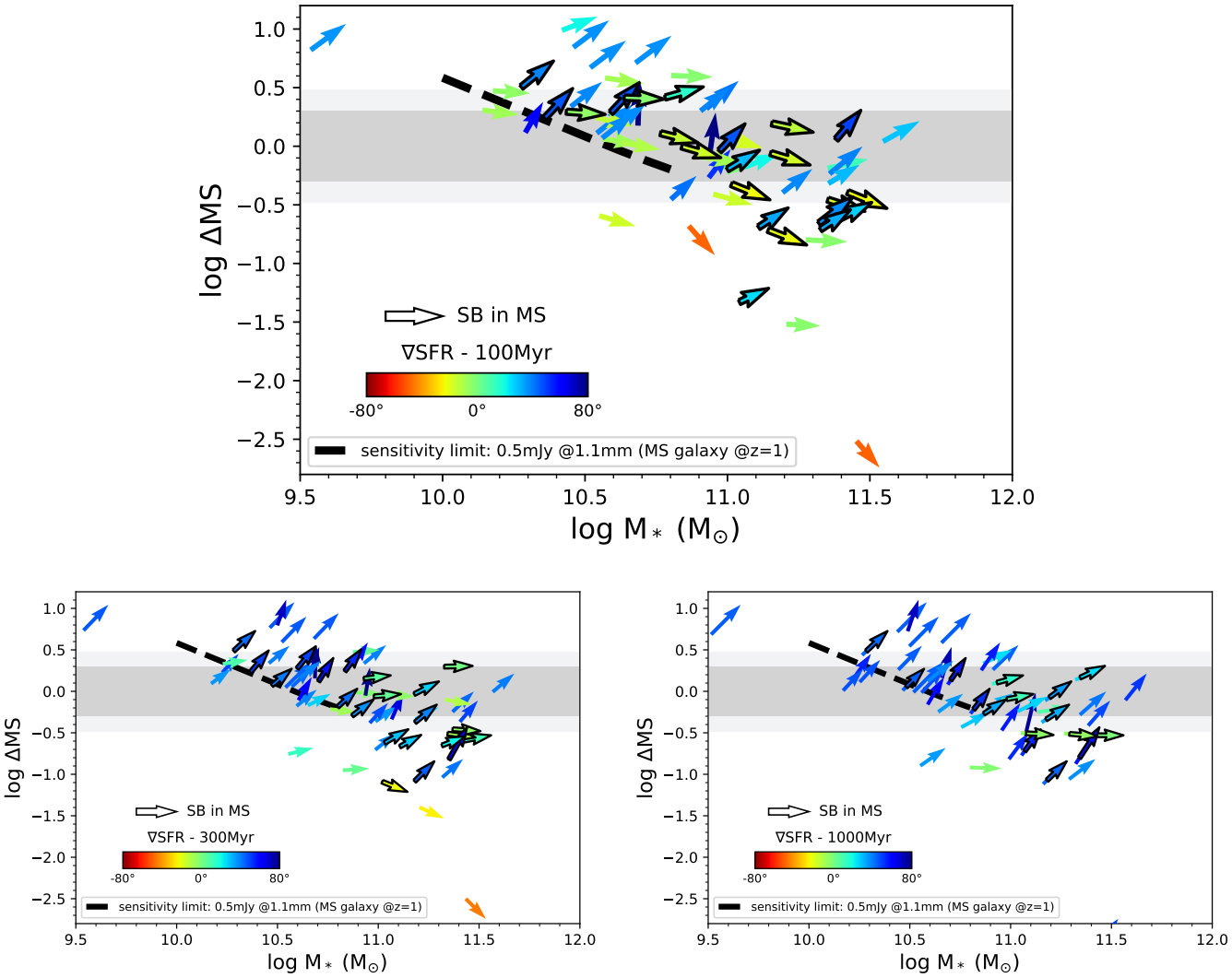

Fig. 6. GOODS-ALMA galaxies, including "SB in the MS" (with black coloured edges), placed on a ΔMS–M_* plane. The assumed MS is from Schreiber et al. (2015). The orientation and colour of the arrows indicate the SFR gradient of each galaxy over a given time: 100 Myr (top panel), 300 Myr (bottom left panel), and 1 Gyr (bottom right panel).

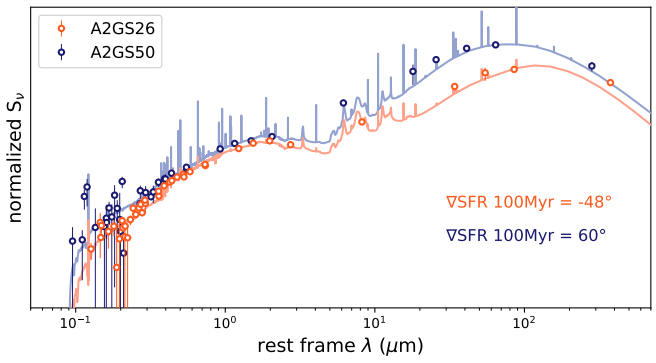

Fig. 7. Example of SED modelling results for two extreme gradient values: A2GS26 (orange) with a SFR gradient over 100 Myr of −48° and A2GS50 (blue) with a gradient of 60° over the same period. Circles are flux densities, while solid lines are the best fits. The SEDs are normalised to their rest-frame 2 μm flux densities, which is a proxy for stellar mass.

In the GOODS-ALMA sample, only two galaxies have a very low gradient indicative of a rapid decline in star formation, which would be expected if a galaxy became rapidly passive. All the GOODS-ALMA galaxies have a gradient of higher than −50°, as shown in the left panels of Fig. 9; their last 100 Myr of SFH do not show any evidence of a rapid decline in star-formation activity that could have followed a strong starburst phase where the galaxies could have lied above the MS. Over a longer timescale of 300 Myr, arrows indicate mostly an increasing SF activity, with a few galaxies having a flatter arrow and decreasing activity. When the gradients are computed over 1 Gyr, almost all of the galaxies have an increasing gradient, meaning that overall, the SF activity of the GOODS-ALMA galaxies has increased over the last 1 Gyr. We note that several galaxies do not have an estimate of the gradient over 1 Gyr due to the fact that the age resulting from the SED fitting is lower. Over these two timescales (300 Myr and 1 Gyr), no strong decline in the SFH of the GOODS-ALMA galaxies is observed through their SFR gradient.

In Fig. 6, the compact galaxies, called 'SB in the MS', do not show any specific trend compared to the other GOODS-ALMA galaxies. To verify this, we show in Fig. 9 the 100, 300, and 1000 Myr gradient distributions of both 'SB in the MS' and the rest of the GOODS-ALMA galaxies, and considering the

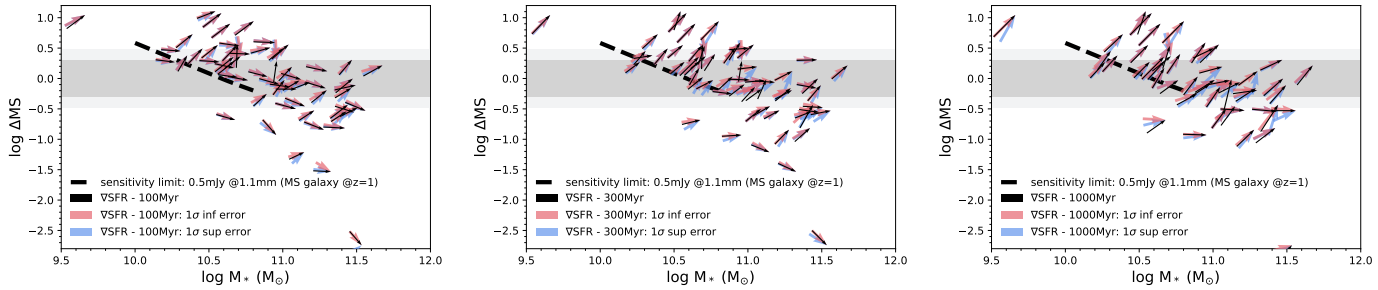

Fig. 8. GOODS-ALMA galaxies, including "SB in the MS", placed on a ΔMS–M_* plane. The assumed MS is from Schreiber et al. (2015). The orientation of the thin black arrows indicates the SFR gradient of each galaxy over a given time: 100 Myr (left panel), 300 Myr (middle panel), and 1 Gyr (right panel). The red and blue arrows represent the upper (blue) and lower (red) 1σ error on the gradient estimates.

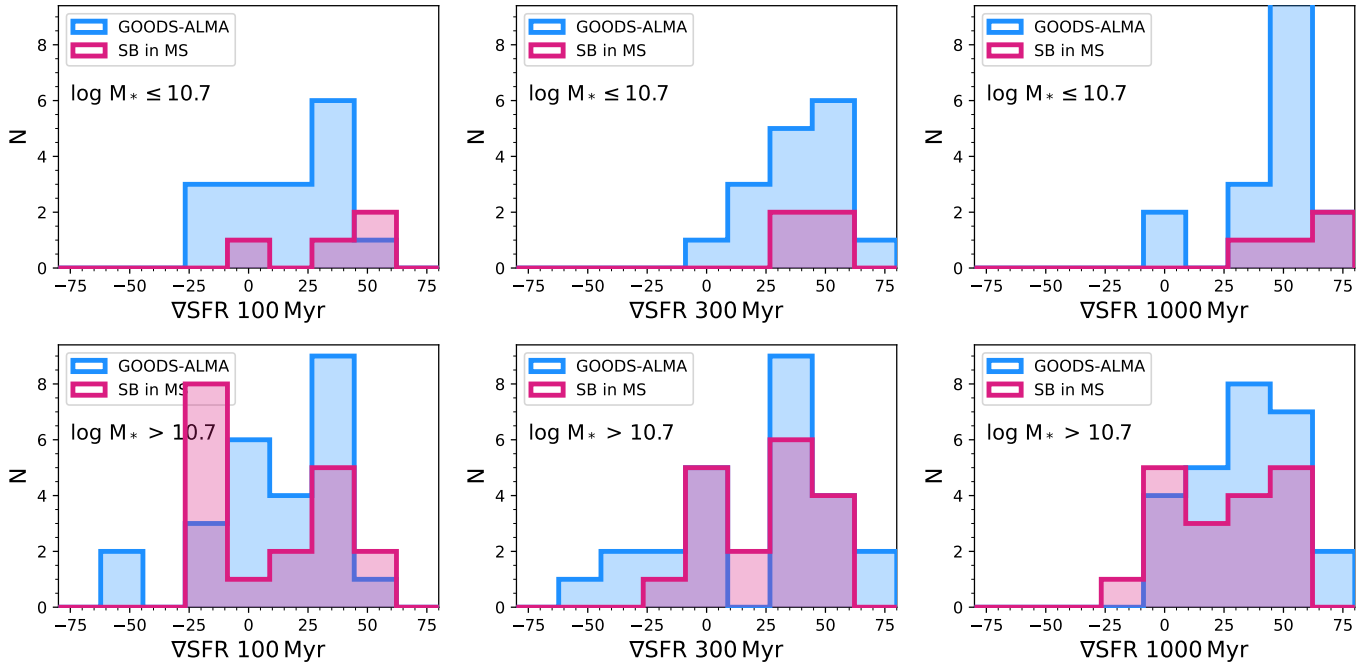

Fig. 9. Histograms of the SFR gradients measured at 100, 300, and 1000 Myr for the GOODS-ALMA galaxies classified as starbursts in the MS (red) and the other galaxies of the GOODS-ALMA sample (blue). The top row of panels shows the distribution for galaxies with $\log M_* \leq 10.7$ while the bottom row of panels are galaxies with $\log M_* > 10.7$.

low- (top row) and high-mass (bottom row) groups. For each timescale, there is no significant difference between the gradient distributions of GOODS-ALMA galaxies and SB in the MS, as confirmed by Kolmogorov-Smirnov (KS) tests, which is true for both the low- and high-mass groups. We conclude that the SB in the MS galaxies do not exhibit any particular SFH that could explain their low depletion time compared to the whole GOODS-ALMA sample.

5. Discussion

The aim of this work is to try to distinguish which of the three evolutionary scenarios proposed by Gómez-Guijarro et al. (2022b) can best explain the physical properties of the compact galaxies "SB in the MS". The first scenario was introduced in Tacchella et al. (2016) and is characterised by compaction events triggered by a strong gas inflow. If the gas stream is counter-rotating, or if minor mergers are involved, there is a loss of angular momentum; the inflow rate is more efficient than the SFR, the gas moves to the centre of the galaxy, and a compact massive core of gas grows, yielding a sustained SFR. The compaction phase is characterised by a short depletion time and a high gas fraction. As a consequence, the galaxy moves up to the highest part of the MS. This enhanced star formation activity leads to central gas depletion, and therefore inside-out quenching, and the galaxy moves to the lower part of the MS. If the galaxy resides in a low-mass halo then another compaction event can occur; alternatively, if massive enough, the hot dark matter halo prevents further gas inflow, leading to gas depletion and full quenching. However, Gómez-Guijarro et al. (2022b) ruled out this scenario to explain the properties of 'SBs in the MS", as these authors do not find galaxies characterised by ongoing compact star formation, short depletion times, and high gas fractions located within the scatter of the MS, as predicted in this first scenario in the upper bound of the MS. The favoured scenario is a mechanism that reduces the angular momentum. These latter authors considered two possibilities: one in which the galaxy rises far above the MS (their 'scenario 2') and one where it only mildly rises, remaining within the MS (their 'scenario 3'). The authors note that existing data discussed in this paper do not allow them to clearly distinguish between the two scenarios, while scenario 3 could in principle explain why such compact star formation is

systematically found among high-mass MS galaxies. This evolutionary path, consistent with a slow downfall (Schreiber et al. 2015; Gómez-Guijarro et al. 2019; Franco et al. 2020), would imply that the galaxy is still experiencing the last phases of regulation implied by the MS while it is on its way to quiescence.

In the previous section, we showed that GOODS-ALMA galaxies, and in particular the "SB in the MS" galaxies, do not exhibit very low SFR gradients over the last 100 Myr. Scenario 2 of Gómez-Guijarro et al. (2022b) proposes that the low gas fraction of 'SB in the MS' galaxies can be explained by the fact that the galaxies exhausted their gas reservoir during a strong starburst phase, putting them above the MS. If indeed the 'SB in the MS' galaxies were found to be in the transition between the SB region and the passive one due to gas exhaustion, a very low SFR gradient would be expected for these sources. However, we observe positive or weak negative values for the "SB in the MS" galaxies in the last 100 Myr, which is not compatible with scenario 2. Even considering a larger timescale, that is 300 Myr for instance, no sign of rapid quenching is seen among this population either. This is also confirmed when looking at the last gigayear. Therefore, our study rules out scenario 2 of Gómez-Guijarro et al. (2022b). We note that Fensch et al. (2017) showed that gas-rich mergers do not generate strong starbursts, that is with large sSFR far above the MS, because of their strong internal turbulence, which is provoked by their large gas mass. From this perspective, it is understandable how mergers among gas-rich galaxies within the MS could reduce the angular momentum of the gas without bringing the galaxies far above the MS as in scenario 2. Indeed, it has been claimed that galaxies above the MS at $z \sim 2$ systematically exhibit enhanced gas fractions associated with a mild increase in star formation efficiency (SFE), although this is still debated (e.g., Tacconi et al. 2018). Furthermore, recently, using zoomed-in simulations, Renaud et al. (2022) showed that a short depletion time, which is characteristic of a starburst, is not linked to the sSFR, and does not yield an excess in sSFR compared to MS galaxies.

Selection effects, as introduced in the previous sections, are to be considered. At stellar masses lower than $5 \times 10^{10}\ M_{\odot}$ most of the sample is located in the upper part of the MS. Therefore, we note that the interpretation in this discussion is to be applicable to the high-mass end, under the assumption of gas replenishment being halted or strongly suppressed in hot dark matter haloes, preventing further gas inflow and/or cooling, eventually leading to quenching (e.g., Rees & Ostriker 1977; Birnboim & Dekel 2003; Feldmann & Mayer 2015). Time variations in gas accretion, consumption, feedback, and other physical processes could also be at play, especially at the low-mass end.

We show that "SB in the MS" galaxies do not exhibit different SFHs from the other galaxies of the GOODS-ALMA sample. In other words, these galaxies are not distinguishable from any other GOODS-ALMA galaxies based on their SED and therefore recent SFH. For this reason, we conclude that, despite their different properties (compactness, low depletion time), these sources manage to regulate themselves and stay within the MS; they maintain their star-formation activity despite their lack of gas. The presence of these sources and their ability to self regulate and stay within the MS reveal a more complex picture of the MS than previously thought.

6. Conclusions

With this work, we aim to constrain the recent SFH of the GOODS-ALMA galaxy sample presented in Gómez-Guijarro et al. (2022a; 2022b) in order to put constraints on the different evolutionary scenarios proposed by these latter authors to explain the presence of galaxies with starburst properties lying on the MS, the so-called SB in the MS galaxies.

To conduct this analysis, we included non-parametric SFHs in CIGALE. Based on simulated SFHs, we show that these models provide a better estimate of the stellar mass of galaxies than parametric SFHs, as well as more accurate SFRs. These results confirm the conclusions reached by Lower et al. (2020) and Leja et al. (2021). In this work, we use a 'bursty' continuity prior, as introduced by Tacchella et al. (2021a). We show that the non-parametric SFH is sensitive to strong starburst variations and rapid quenching events, with a slight overestimate of the SFR in the case of strong quenching occurring less than 100 Myr ago. To characterise the SFH, we define the SFR gradient (∇SFR), which indicates the trend of the SFH over a given time by computing the angle between the ΔSFR and ΔM_* variations over this given time. A ∇SFR of close to zero° is obtained for constant SFH, while a value close to +(−)90° indicates a strong starburst (rapid quenching) event.

We selected the 65 GOODS-ALMA galaxies detected with *Herschel* that are not optically dark. We fitted these galaxies with CIGALE using the non-parametric SFHs. GOODS-ALMA galaxies have a $\nabla\mathrm{SFR}_{100}$ ranging from −50° to 75°. The wide distribution of measured $\nabla\mathrm{SFR}_{100}$ is an indicator of the stochasticity of the recent SFH, while the long-term SFH can be observed from $\nabla\mathrm{SFR}_{1000}$.

The "SB in the MS" galaxies have positive to weak negative SFR gradients over the last 100 Myr, which is not compatible with an evolutionary path where these galaxies come from the SB region above the MS. If this latter scenario were true, strong negative gradients would be expected, indicative of a rapid quenching due to gas exhaustion. This result holds even when considering long timescales (300 Myr and 1 Gyr), confirming the absence of rapid quenching over the last gigayear. Therefore, our results rule out the second scenario proposed in Gómez-Guijarro et al. (2022b), where the 'SB in the MS' galaxies could be those transitioning from the SB region to stay on the MS or going through quiescence.

We find no differences in the SFH of the last 1 Gyr between the galaxies classified as SB in the MS by Gómez-Guijarro et al. (2022b) and the other GOODS-ALMA galaxies. Despite their different properties (compactness, low depletion time), the 'SB in the MS' galaxies have a similar SFH to the other GOODS-ALMA galaxies and cannot be identified from their SED, and therefore their SFH. In other words, these galaxies manage a form of self regulation, maintaining their star-formation activity, allowing them to stay within the MS despite their lack of gas. The particularities of this subpopulation highlight a diversity within the MS, suggesting more complexity within the relation than previously thought.

Acknowledgements. L.C. warmly thanks M. Boquien and Y. Roehlly for their help in implementing the non-parametric SFHs in CIGALE and O. Ilbert for useful discussions. This project has received financial support from the CNRS through the MITI interdisciplinary programs. S.J. acknowledges the Villum Fonden research grants 37440, 13160 and the financial support from European Union's Horizon research and innovation program under the Marie Skłodowska-Curie grant agreement No. 101060888. M.F. acknowledges NSF grant AST-2009577 and NASA JWST GO Program 1727. H.I. acknowledges support from JSPS KAKENHI Grant Number JP19K23462. G.E.M. acknowledges the Villum Fonden research grants 13160 and 37440 and the Cosmic Dawn Center of Excellence funded by the Danish National Research Foundation under the grant No. 140.

References

Aufort, G., Ciesla, L., Pudlo, P., & Buat, V. 2020, A&A, 635, A136

Benson, A. J., & Bower, R. 2010, MNRAS, 405, 1573
Birnboim, Y., & Dekel, A. 2003, MNRAS, 345, 349
Boquien, M., Burgarella, D., Roehlly, Y., et al. 2019, A&A, 622, A103
Bower, R. G., Benson, A. J., Malbon, R., et al. 2006, MNRAS, 370, 645
Bruzual, G., & Charlot, S. 2003, MNRAS, 344, 1000
Buat, V., Heinis, S., Boquien, M., et al. 2014, A&A, 561, A39
Buat, V., Oi, N., Heinis, S., et al. 2015, A&A, 577, A141
Buat, V., Ciesla, L., Boquien, M., Małek, K., & Burgarella, D. 2019, A&A, 632, A79
Calzetti, D., Armus, L., Bohlin, R. C., et al. 2000, ApJ, 533, 682
Carnall, A. C., McLure, R. J., Dunlop, J. S., & Davé, R. 2018, MNRAS, 480, 4379
Carnall, A. C., Leja, J., Johnson, B. D., et al. 2019, ApJ, 873, 44
Ciesla, L., Charmandaris, V., Georgakakis, A., et al. 2015, A&A, 576, A10
Ciesla, L., Elbaz, D., & Fensch, J. 2017, A&A, 608, A41
Ciesla, L., Elbaz, D., Schreiber, C., Daddi, E., & Wang, T. 2018, A&A, 615, A61
Ciesla, L., Buat, V., Boquien, M., et al. 2021, A&A, 653, A6
Cole, S., Lacey, C. G., Baugh, C. M., & Frenk, C. S. 2000, MNRAS, 319, 168
Dale, D. A., Helou, G., Magdis, G. E., et al. 2014, ApJ, 784, 83
Dekel, A., Zolotov, A., Tweed, D., et al. 2013, MNRAS, 435, 999
Dickinson, M., Giavalisco, M., & GOODS Team 2003, in The Mass of Galaxies at Low and High Redshift, eds. R. Bender, & A. Renzini , 324
Elbaz, D., Daddi, E., Le Borgne, D., et al. 2007, A&A, 468, 33
Elbaz, D., Dickinson, M., Hwang, H. S., et al. 2011, A&A, 533, A119
Elbaz, D., Leiton, R., Nagar, N., et al. 2018, A&A, 616, A110
Feldmann, R., & Mayer, L. 2015, MNRAS, 446, 1939
Fensch, J., Renaud, F., Bournaud, F., et al. 2017, MNRAS, 465, 1934
Franco, M., Elbaz, D., Béthermin, M., et al. 2018, A&A, 620, A152
Franco, M., Elbaz, D., Zhou, L., et al. 2020, A&A, 643, A30
Giavalisco, M., Ferguson, H. C., Koekemoer, A. M., et al. 2004, ApJ, 600, L93
Gómez-Guijarro, C., Toft, S., Karim, A., et al. 2018, ApJ, 856, 121
Gómez-Guijarro, C., Magdis, G. E., Valentino, F., et al. 2019, ApJ, 886, 88
Gómez-Guijarro, C., Elbaz, D., Xiao, M., et al. 2022a, A&A, 658, A43
Gómez-Guijarro, C., Elbaz, D., Xiao, M., et al. 2022b, A&A, 659, A196
Guo, K., Zheng, X. Z., & Fu, H. 2013, ApJ, 778, 23
HerMES Collaboration (Oliver, S. J., et al.) 2012, MNRAS, 424, 3
Hopkins, P. F., Hernquist, L., Cox, T. J., et al. 2006, ApJS, 163, 1
Iyer, K., & Gawiser, E. 2017, ApJ, 838, 127
Iyer, K. G., Gawiser, E., Faber, S. M., et al. 2019, ApJ, 879, 116
Jiménez-Andrade, E. F., Magnelli, B., Karim, A., et al. 2019, A&A, 625, A114
Johnson, B. D., Leja, J., Conroy, C., & Speagle, J. S. 2021, ApJS, 254, 22
Khusanova, Y., Bethermin, M., Le Fèvre, O., et al. 2021, A&A, 649, A152
Leja, J., Johnson, B. D., Conroy, C., van Dokkum, P. G., & Byler, N. 2017, ApJ, 837, 170
Leja, J., Carnall, A. C., Johnson, B. D., Conroy, C., & Speagle, J. S. 2019, ApJ, 876, 3
Leja, J., Speagle, J. S., Ting, Y.-S., et al. 2021, ApJ, 936, 18
Lower, S., Narayanan, D., Leja, J., et al. 2020, ApJ, 904, 33
Lutz, D., Poglitsch, A., Altieri, B., et al. 2011, A&A, 532, A90
Magdis, G. E., Daddi, E., Béthermin, M., et al. 2012, ApJ, 760, 6
Magnelli, B., Popesso, P., Berta, S., et al. 2013, A&A, 553, A132
Małek, K., Buat, V., Roehlly, Y., et al. 2018, A&A, 620, A50
Merlin, E., Castellano, M., Santini, P., et al. 2021, A&A, 649, A22
Mihos, J. C., & Hernquist, L. 1996, ApJ, 464, 641
Noeske, K. G., Weiner, B. J., Faber, S. M., et al. 2007, ApJ, 660, L43
Ocvirk, P., Pichon, C., Lançon, A., & Thiébaut, E. 2006, MNRAS, 365, 46
Puglisi, A., Daddi, E., Valentino, F., et al. 2021, MNRAS, 508, 5217
Rees, M. J., & Ostriker, J. P. 1977, MNRAS, 179, 541
Renaud, F., Segovia Otero, Á., & Agertz, O. 2022, MNRAS, 516, 4922
Saintonge, A., & Catinella, B. 2022, ARA&A, 60, 319
Salmi, F., Daddi, E., Elbaz, D., et al. 2012, ApJ, 754, L14
Salpeter, E. E. 1955, ApJ, 121, 161
Schreiber, C., Pannella, M., Elbaz, D., et al. 2015, A&A, 575, A74
Schreiber, C., Glazebrook, K., Nanayakkara, T., et al. 2018a, A&A, 618, A85
Schreiber, C., Labbé, I., Glazebrook, K., et al. 2018b, A&A, 611, A22
Seillé, L. M., Buat, V., Haddad, W., et al. 2022, A&A, 665, A137
Speagle, J. S., Steinhardt, C. L., Capak, P. L., & Silverman, J. D. 2014, ApJS, 214, 15
Suess, K. A., Leja, J., Johnson, B. D., et al. 2022, ApJ, 935, 146
Tacchella, S., Dekel, A., Carollo, C. M., et al. 2016, MNRAS, 458, 242
Tacchella, S., Forbes, J. C., & Caplar, N. 2020, MNRAS, 497, 698
Tacchella, S., Conroy, C., Faber, S. M., et al. 2021a, ApJ, 926, 36
Tacchella, S., Finkelstein, S. L., Bagley, M., et al. 2021b, ApJ, 927, 29
Tacconi, L. J., Genzel, R., Saintonge, A., et al. 2018, ApJ, 853, 179
Toft, S., Smolčić, V., Magnelli, B., et al. 2014, ApJ, 782, 68
Topping, M. W., Stark, D. P., Endsley, R., et al. 2022, MNRAS, 516, 975
Wuyts, S., Förster Schreiber, N. M., van der Wel, A., et al. 2011, ApJ, 742, 96
Zolotov, A., Dekel, A., Mandelker, N., et al. 2015, MNRAS, 450, 2327